Climate–Carbon Cycle Feedback Analysis: Results from the C[4]MIP Model Intercomparison

P. Friedlingstein,[a] P. Cox,[b] R. Betts,[c] L. Bopp,[a] W. von Bloh,[d] V. Brovkin,[d] P. Cadule,[e]
S. Doney,[f] M. Eby,[g] I. Fung,[h] G. Bala,[i] J. John,[h] C. Jones,[c] F. Joos,[j] T. Kato,[k] M. Kawamiya,[k]
W. Knorr,[l] K. Lindsay,[m] H. D. Matthews,[g,n] T. Raddatz,[o] P. Rayner,[a] C. Reick,[o] E. Roeckner,[p]
K.-G. Schnitzler,[p] R. Schnur,[p] K. Strassmann,[j] A. J. Weaver,[g] C. Yoshikawa,[k] and N. Zeng[q]

[a] IPSL/LSCE, Gif-sur-Yvette, France
[b] Centre for Ecology and Hydrology, Dorchester, United Kingdom
[c] Hadley Centre, Met Office, Exeter, United Kingdom
[d] Potsdam Institute for Climate Impact Research, Potsdam, Germany
[e] CNRS/IPSL, Paris, France
[f] Woods Hole Oceanographic Institution, Woods Hole, Massachusetts
[g] University of Victoria, Victoria, British Columbia, Canada
[h] University of California, Berkeley, Berkeley, California
[i] Lawrence Livermore National Laboratory, Livermore, California
[j] University of Bern, Bern, Switzerland
[k] Frontier Research Center for Global Change/JAMSTEC, Yokohama, Japan
[l] QUEST, University of Bristol, Bristol, United Kingdom
[m] NCAR, Boulder, Colorado
[n] University of Calgary, Calgary, Alberta, Canada
[o] Max Planck Institute for Biogeochemistry, Jena, Germany
[p] Max Planck Institute for Meteorology, Hamburg, Germany
[q] University of Maryland, College Park, College Park, Maryland

ABSTRACT

Eleven coupled climate–carbon cycle models used a common protocol to study the coupling between climate change and the carbon cycle. The models were forced by historical emissions and the Intergovernmental Panel on Climate Change (IPCC) Special Report on Emissions Scenarios (SRES) A2 anthropogenic emissions of CO_2 for the 1850–2100 time period. For each model, two simulations were performed in order to isolate the impact of climate change on the land and ocean carbon cycle, and therefore the climate feedback on the atmospheric CO_2 concentration growth rate. There was unanimous agreement among the models that future climate change will reduce the efficiency of the earth system to absorb the anthropogenic carbon perturbation. A larger fraction of anthropogenic CO_2 will stay airborne if climate change is accounted for. By the end of the twenty-first century, this additional CO_2 varied between 20 and 200 ppm for the two extreme models, the majority of the models lying between 50 and 100 ppm. The higher CO_2 levels led to an additional climate warming ranging between 0.1° and 1.5°C.

All models simulated a negative sensitivity for both the land and the ocean carbon cycle to future climate. However, there was still a large uncertainty on the magnitude of these sensitivities. Eight models attributed most of the changes to the land, while three attributed it to the ocean. Also, a majority of the models located the reduction of land carbon uptake in the Tropics. However, the attribution of the land sensitivity to changes in net primary productivity versus changes in respiration is still subject to debate; no consensus emerged among the models.

Corresponding author address: Pierre Friedlingstein, Institut Pierre-Simon Laplace/Laboratoire des Sciences du Climat et de l'Environnement, CEA-Saclay, L'Orme des Merisiers, 91191 Gif-sur-Yvette, France.
E-mail: pierre.friedlingstein@cea.fr

1. Introduction

Atmospheric CO_2 concentration is one of the most important factors likely to determine the climate of the twenty-first century (Houghton et al. 2001). In projecting the future climate changes, the majority of experiments with comprehensive ocean–atmosphere general circulation models (OAGCMs) still use prescribed CO_2 concentration scenarios, derived using relatively simple offline carbon cycle models. Although these carbon cycle models may account for the carbon cycle response to climate change (e.g., the Bern model in Prentice et al. 2001), this approach is still not fully consistent. First, the carbon cycle models use a prescribed climate change pattern to calculate the carbon fluxes and the atmospheric CO_2 for a given emission scenario; then the resulting atmospheric CO_2 trajectory is used to drive OAGCMs in order to calculate a climate change. There is no guarantee that the resulting climatology of the climate change from the OAGCM is similar in amplitude and spatial pattern to the one applied to the offline carbon cycle model. The resulting climate projections inevitably suffer from inconsistencies between the comprehensive physical climate models and the carbon models. The atmosphere–land and atmosphere–ocean fluxes of CO_2 are known to be sensitive to climate. For example, the growth rate of atmospheric CO_2 varies with the El Niño–Southern Oscillation (e.g., Bousquet et al. 2000), and is also believed to have been affected by the climate perturbation arising from the Pinatubo volcanic eruption (Jones and Cox 2001; Lucht et al. 2002).

In the context of future climate change, offline carbon cycle simulations have been extensively performed (e.g., Prentice et al. 2001). For example, Cramer el al. (2001), compared the response of six dynamic global vegetation models when forced by a future climate scenario projected by the Hadley Centre Coupled Model version 2 (HadCM2) model and a prescribed CO_2 trend. Simulations including climate change showed a reduced terrestrial carbon sink in all models as a result of the impacts of climate change on net ecosystem productivity (NEP) of tropical and Southern Hemisphere ecosystems. Two recent studies by Berthelot et al. (2005) and Ito (2005) each used one terrestrial carbon cycle model forced by several future climate scenarios taken from different OAGCMs. Again, both studies showed, regardless of the climate model used, a reduction of carbon uptake with climate change. Similarly, ocean studies have been performed with imposed atmospheric CO_2 trajectories. Projected changes in sea surface temperature and oceanic circulation lead to a reduction of carbon uptake (e.g., Sarmiento et al. 1998; Chuck et al. 2005).

Since an increase in CO_2 leads to climatic change, and climatic change in turn affects the CO_2 concentration, the climate, atmospheric CO_2, and the carbon cycle form a feedback loop. The first two OAGCM climate projections to include an interactive carbon cycle showed that the climate–carbon cycle feedback is positive (i.e., amplifying externally induced perturbation) mostly due to the negative impacts of climate change on land carbon storage (Cox et al. 2000; Friedlingstein et al. 2001; Dufresne et al. 2002). But the magnitude of the feedback varied markedly between the results from the Hadley Centre and L'Institut Pierre-Simon Laplace (IPSL) models (Friedlingstein et al. 2003). In the context of the Coupled Climate–Carbon Cycle Model Intercomparison Project (C^4MIP; Fung et al. 2000; Cox et al. 2002), seven coupled OAGCMs and four models of intermediate complexity performed coupled climate–carbon cycle simulations over the historical period and the twenty-first century (Table 1). All models used observed anthropogenic fossil fuel emissions for the historical period (Marland et al. 2005) and the Intergovernmental Panel on Climate Change (IPCC) Special Report on Emissions Scenarios (SRES) A2 emission scenario for the 2000–2100 period.

Most models included land-use-associated CO_2 emissions provided by Houghton and Hackler (2002) for the historical and by the Integrated Model to Assess the Global Environment (IMAGE)-integrated model for the twenty-first century (Leemans et al. 1998). However, none of the models prescribed actual land-cover changes as boundary conditions of the vegetation model. Changes in physical and biogeochemical properties of the vegetation following land-cover changes were hence neglected in this study. Land-use-associated emissions are seen here as an external forcing. Each modeling group carried out at least two simulations, one "coupled" simulation in which climate change affects the carbon cycle, and one "uncoupled" simulation in which CO_2 is treated as a nonradiatively active gas (so that the carbon cycle experiences no CO_2-induced climate change). The difference between these two runs defines the effect of climate on carbon cycle and hence on atmospheric CO_2 that is fundamental for the climate–carbon feedback.

2. Model description

The 11 C^4MIP models are briefly described here. Table 1 summarizes the main characteristics of the models.

HadCM3LC couples the HadCM3 (Gordon et al. 2000) to an ocean and a terrestrial carbon cycle model.

TABLE 1. Major characteristics of the C⁴MIP models components.

Models	Atmosphere	Ocean	Land carbon	DGVM	Ocean carbon	References
HadCM3LC	HADCM3 2.5° × 3.75°, L19	2.5° × 3.75°, L20 flux adjustment	MOSES/TRIFFID	Yes	HadOCC	Cox et al. (2000)
IPSL-CM2C	LMD5 64 × 50, L19 (5° × 4°)	OPA-7, 2° × 2°, L31 no flux adjustment	SLAVE	No	NPZD	Dufresne et al. (2002)
IPSL-CM4-LOOP	LMDZ-4 96 × 72, L19 (3° × 3)	ORCA2, 2° × 2°, L31, no flux adjustment	ORCHIDEE	Not here	PISCES	Marti et al. (2005) Krinner et al. (2005) Aumont et al. (2003)
CSM-1	CCM3 T31, L18	NCOM 3.6 ° lon 0.8–1.8 ° lat	LSM, CASA	No	OCMIP-biotic	Doney et al. (2006); Fung et al. (2005)
MPI	ECHAM5, T63, L31	MPI-OM, 1.5 °, L40, no flux adjustment	JSBACH	No	HAMOCC5	Raddatz et al. (2005, unpublished manuscript)
LLNL	CCM3, 2.8° × 2.8°, L18	POP 0.6 ° × 0.6 °, L40	IBIS, flux adjustment	Yes	OCMIP	Thompson et al. (2004)
FRCGC	CCSR/NIES/FRCGC T42(2.8° × 2.8°), L20	COCO No flux adjustment, (0.5°–1.4°) × 1.4°, L20	Sim-CYCLE	No	NPZD	
UMD	QTCM 5.6° × 3.7°	Slab mixed layer, 5.6° × 3.7°	VEGAS	Yes	Three-box model	Zeng et al. (2004)
UVic-2.7	EMBM 1.8° × 3.6°	Mom 2.2, 1.8° × 3.6°, L19, no flux adjustment	MOSES/TRIFFID	Yes	OCMIP Abiotic	Meissner et al. (2003) Matthews et al. (2005a)
CLIMBER2-LPJ	2.5-D, 10° × 51° statistical-dynamical	Zonally averaged, 2.5°lat, 3 basins	LPJ	Yes	NPZD	Brovkin et al. (2004) Sitch et al. (2005)
BERN-CC	EBM 2.5° × 3.75°	HILDA box-diffusion model	LPJ	Yes	Perturbation approach	Joos et al. (2001) Gerber et al. (2003)

Both atmosphere and ocean components use a horizontal resolution of 2.5° latitude × 3.75° longitude, and the model requires the use of flux adjustments (Johns et al. 1997). The dynamic global vegetation model, Top-Down Representation of Interactive Foliage and Flora including Dynamics (TRIFFID; Cox 2001), coupled to the land surface scheme, Met Office Surface Exchange Scheme (MOSES; Cox et al. 1999), simulates the carbon uptake of, and competition between, five functional types: broadleaf tree, needleleaf tree, C3 grass, C4 grass, and shrubs. Stomatal conductance and photosynthesis are calculated via a coupled leaf-level model, with leaf area index estimated from a percentage of the whole-plant carbon balance. Net primary productivity (NPP) is the difference between the simulated photosynthesis and dark respiration, with photosynthesis coupled to transpiration (Collatz et al. 1991, 1992). NPP increases with CO_2 and also responds to temperature, photosynthetically active radiation (PAR), humidity, and soil moisture stress (Cox 2001). Organic matter in the single soil carbon pool decomposes at a rate determined by soil temperature (with Q10 = 2) and soil moisture (with maximal decomposition at an optimal soil moisture; McGuire et al. 1992). The Hadley Centre ocean carbon cycle model (HadOCC; Palmer and Totterdell 2001) contains a four-component nutrient–phytoplankton–zooplankton–detritus (NPZD) ecosystem model that simulates the effects of light penetration, alkalinity, and (nitrate) nutrient availability on the biological carbon uptake.

The IPSL–CM2C is based on the IPSL–CM2 physical ocean–atmosphere GCM (Khodri et al. 2001). The atmospheric model has a resolution of about 400 × 400 km at 50°N. The ocean model spatial resolution over high latitude reaches a maximum size of 4° by 3°. The terrestrial carbon model [Scheme for Large-Scale Atmosphere Vegetation Exchange (SLAVE); Friedlingstein et al. 1995] calculates NPP following a light use efficiency formulation (Field et al. 1995) that is a function of temperature and water stress. NPP increases with CO_2 under a Michaelis–Menten beta factor formulation. The models is composed of two litter pools, a fast and a slow soil carbon pool, following the rational of the CENTURY model (Parton et al. 1993). Organic matter decomposition is controlled by temperature using a Q10 formulation and by soil moisture stress. The ocean carbon model is HAMOCC3 (Maier-Reimer 1993; Aumont et al. 1999). This model computes the fluxes resulting from the biological activity rather than describing this biological activity itself. Export production is assumed proportional to the local phosphate concentration but is modulated by light, temperature, mixed-layer depth, and abundance of nutrients. Or-

ganic matter and calcareous tests instantaneously sink below the euphotic zone according to prescribed vertical profiles.

The IPSL–CM4–LOOP model couples the latest version of the IPSL ocean–atmosphere GCM (Marti et al. 2005) used for the IPCC AR4 simulations (Dufresne et al. 2005) to the land carbon cycle model, Organizing Carbon and Hydrology in Dynamic Ecosystems (ORCHIDEE; Krinner et al. 2005) and ocean carbon cycle model, Pelagic Iteraction Scheme for Carbon and Ecosystem Studies (PISCES; Aumont et al. 2003). The Laboratoire de Météorologie Dynamique atmospheric model (LMDZ-4) has a horizontal resolution of about 3° × 3°, with 19 vertical levels (Hourdin et al. 2005). The ORCALIM ocean and sea ice model has a resolution of 0.5°–2° with 31 vertical levels in the ocean (Madec et al. 1998). No flux correction is applied. ORCHIDEE is a global vegetation model that calculates the energy and hydrology budgets, carbon assimilation, allocation, and decomposition for 13 plant functional types (PFTs). It uses the Farquhar et al. (1980) and Collatz et al. (1992) C_3 and C_4 photosynthesis model and the Ball et al. (1986) and Collatz et al. (1991, 1992) formulations for stomatal conductance. Allocation between eight living carbon pools is based on Friedlingstein et al. (1999). The model accounts for four litter pools and three (fast, slow, and passive) soil carbon pools. Organic matter decomposition is dependent on soil moisture and soil temperature using a Q10 dependence, where Q10 = 2. PISCES is a global ocean carbon model that includes a simple marine ecosystem model, with four plankton functional groups (nanophytoplankton, diatoms, microzooplankton, and mesoplankton). Nutrient colimitation of phytoplankton growth is a function of N, P, Si, and Fe. The iron cycle is explicitly modeled including input from atmospheric dust and coastal sediments. In the water column, sinking of particulate carbon is explicitly considered using a simple two-size-class model for the particulate organic carbon.

The Climate System Model version 1 (CSM-1; Doney et al. 2006) is based on the National Center for Atmospheric Research (NCAR) CSM1.4, which consists of three-dimensional ocean and atmosphere GCMs, a land biogeophysics package, and a sea ice component (Boville and Gent 1998; Boville et al. 2001). The horizontal resolution of the atmosphere and land models is T31 (~3.75°). The atmosphere has 10 levels in the troposphere and 8 levels in the stratosphere. The ocean and sea ice modules have a horizontal resolution of 0.8°–1.8° in latitude and 3.6° in longitude. The ocean has 25 vertical levels. The physical model does not use flux correction. The land component of CSM1.4,

LSM1.0 (Bonan 1996), has six soil layers extending to 6.3 m. Each model grid box contains fractional coverage by up to 3 PFTs from a total of 13 PFTs (including bare ground). The terrestrial carbon model, Carnegie–Ames–Stanford approach (CASA; Randerson et al. 1997) takes carbon assimilation, or gross primary productivity (GPP), each 20-min time step for each PFT from the Land Surface Model (LSM). GPP is climate dependent and increases with CO_2 through limiting assimilation via the Rubisco enzyme as a function of internal leaf CO_2 concentration. CASA consists of up to three live vegetation pools and nine soil pools, with the rates of carbon transfer among them being climate dependent (Dickinson et al. 1998; Friedlingstein et al. 1999). Organic matter decomposition is dependent on soil moisture and soil temperature using a Q10 dependence, where Q10 = 2. Additionally, the carbon cycle is coupled to the water cycle via transpiration, and to the energy cycle via dynamic leaf phenology (and hence albedo). The ocean carbon model is a modified version of the Ocean Carbon-Cycle Model Intercomparison Project version 2 (OCMIP-2) biogeochemistry model (Najjar et al. 1992; Doney et al. 2003). As in the OCMIP-2 model, biota are not explicitly modeled. However, new/export production depends on light, temperature, phosphate, and iron concentrations. The iron cycle includes atmospheric dust deposition/iron dissolution, biological uptake, vertical particle transport, and scavenging.

The Max Planck Institute for Meteorology (MPI) model is based on a coupled ocean–atmosphere GCM as described in Jungclaus et al. (2006). It consists of the atmosphere model ECHAM5 (Roeckner et al. 2003) with a spectral resolution of T63 (1.875° × 1.875°) and 31 vertical levels as well as the MPI ocean model (MPI-OM) with an average horizontal grid spacing of 1.5° and 40 vertical levels (Marsland et al. 2003). No flux adjustment is applied to the physical part of the model. Terrestrial carbon is treated by the modular land surface scheme Joint Scheme for Biosphere Atmosphere Coupling in Hamburg (JSBACH), which is based on the biosphere model Biosphere Energy Transfer and Hydrology scheme (BETHY; Knorr 2000). It includes a photosynthesis scheme following Collatz et al. (1992) for C_4 and Farquhar et al. (1980) for C_3 plants comprising a strong dependence of productivity on atmospheric CO_2 concentration. Additionally stomatal conductance is sensitive to the CO_2 concentration of the ambient air. Soil carbon is partioned in a pool with a short (~1 yr) and one with a long (~100 yr) turnover time. Heterotrophic respiration increases linearly with soil moisture and exponentially with soil temperature (Q10 = 1.5). The carbon cycle within the ocean is simulated by the biogeochemistry model Hamburg Ocean Carbon Cycle Model (HAMOCC5; Wetzel et al. 2005), which includes phyto- and zooplankton dynamics depending on temperature, solar radiation, and turbulence. Nutrients (phosphate, nitrogen, and iron) and the sedimentation of organic carbon are considered.

The physical ocean–atmosphere model of the Lawrence Livermore National Laboratory (LLNL) climate–carbon is the NCAR Department of Energy (DOE) Parallel Climate Transitional Model (PCTM; Washington et al. 2000; Meehl et al. 2004), which is a version of the NCAR CCM 3.2 model (Kiehl et al. 1996) coupled to the LANL Parallel Ocean Program (POP) ocean model (Maltrud et al. 1998). It does not use flux correction. The terrestrial biosphere model is the Integrated Biosphere Simulator (IBIS) version 2 (Foley et al. 1996; Kucharik et al. 2000) and the ocean biogeochemistry model is based on the OCMIP biotic protocols (Najjar and Orr 1999). The horizontal resolution of the land and atmosphere models is approximately 2.8° latitude and 2.8° longitude. The ocean model has a horizontal resolution of (2/3)°. The atmosphere and ocean models have 18 and 40 levels in the vertical, respectively. The physical climate model PCTM does not use flux correction. However, there is a precipitation, correction over the land in order to have a realistic vegetation distribution as discussed in Govindasamy et al. (2005). IBIS uses the Farquhar et al. (1980) and Collatz et al. (1992) photosynthesis model and the Ball et al. (1986) and Collatz et al. (1991, 1992) formulations for stomatal conductance. The annual carbon balance of vegetation is used to predict changes in the leaf area index and biomass for each of 12 plant functional types, which compete for light and water using different ecological strategies. IBIS also simulates carbon cycling through litter and soil organic matter. Microbial activity is dependent on an Arrhenius function of soil temperatures (Lloyd and Taylor 1994) and water-filled pore space. The nitrogen cycle and other nutrient limitations are not represented in IBIS. The ocean biogeochemistry model predicts air–sea CO_2 fluxes, biogenic export of organic matter and calcium carbonate, and distributions of dissolved inorganic carbon, phosphate, oxygen, alkalinity, and dissolved organic matter. The export formulation for biogenic materials is based on that of Maier-Reimer (1993).

The Frontier Research Center for Global Change (FRCGC) model uses the coupled atmosphere–ocean Model for Interdisciplinary Research on Climate (MIROC), in which the Center for Climate System Research–National Institute for Environmental Studies (CCSR–NIES) FRCGC atmospheric GCM is coupled to the CCRS Ocean Component Model (COCO)

OGCM (Hasumi and Emori 2004). The atmospheric resolution is $2.8° \times 2.8°$, with 20 vertical levels, while the ocean resolution is $0.5°–1.4°$ latitude and $1.4°$ longitude with 44 vertical layers including a bottom boundary layer. Flux adjustment is not adopted for coupling. The terrestrial carbon cycle model, Simulation Model of Carbon Cycle in Land Ecosystems (Sim-CYCLE) (Ito and Oikawa 2002), estimates gross primary productivity (GPP) by scaling up a couple of physiological processes (e.g., stomatal conductance and quantum yield) from the single-leaf level to canopy level, on the basis of the dry-matter production theory established by Monsi and Saeki (1953, 2005). GPP increases with CO_2 concentration mainly due to enhanced quantum efficiency and light-saturated photosynthetic rate. Soil organic carbon is divided into two components: a labile and a stable part. Their decomposing rates are calculated by an Arrhenius-type function of soil temperature (Lloyd and Taylor 1994) and an optimal function of soil moisture including depression under dry and water-logged conditions. The ocean carbon cycle model is the four-compartment ecosystem model by Oschlies (2001) with the carbonate system formulation recommended by OCMIP. The ecosystem model describes time evolution of nitrate, phytoplankton, zooplankton, and detritus. Phytoplankton growth depends on light, temperature, and nitrate concentration. Detritus sinks out of the surface layer with a speed of 5 m/d above 200-m depth, below which the vertical profile of sinking flux is prescribed by the Martin et al. (1987) curve.

The University of Maryland (UMD) Coupled Atmosphere–Biosphere–Ocean (CABO) model is an earth system model with simplified physical climate components including the global version of the atmospheric model quasi-equilibrium tropical circulation (QTCM) model (Neelin and Zeng 2000; Zeng et al. 2000), the simple-land model (Zeng et al. 2000), and a slab mixed layer ocean model with Q-flux to represent the effects of ocean dynamics (Hansen et al. 1984). The mixed layer ocean depth is the annual mean derived from Levitus et al. (2000). All models were run at $5.6° \times 3.7°$ horizontal resolution, limited by the resolution of the atmospheric model. The terrestrial carbon model Vegetation–Global–Atmosphere–Soil (VEGAS; Zeng 2003; Zeng et al. 2004, 2005) is a dynamic vegetation model with full soil carbon dynamics. Competition among four plant functional types is determined by climatic constraints and resource allocation strategy such as temperature tolerance and height-dependent shading. Phenology is simulated dynamically as the balance between growth and respiration/turnover. There are three soil carbon pools: fast, intermediate, and slow. The two lower soil pools have weaker temperature de-

pendence of decomposition due to physical protection underground (Q10 value of 2.2 for the fast pool, 1.35 for the intermediate pool, and 1.1 for the slow pool). The fast soil pool uses surface air temperature while the other two uses soil temperature. A three-box ocean carbon model including surface ocean, deep ocean, and sediment component, with parameter values fitted to the Hamburg Ocean Carbon Cycle Model (HAMOCC; Heinze and Maier-Reimer 1999), was coupled to the terrestrial model through a fully mixed atmosphere. No ocean biology is included in the model.

The University of Victoria (UVic) Earth System Climate Model (ESCM) consists of a vertically integrated, energy–moisture balance, atmospheric model, coupled to the Modular Ocean Model version 2 (MOM2) ocean general circulation model and a dynamic–thermodynamic sea ice model (Weaver et al. 2001). The horizontal resolution is $1.8° \times 3.6°$ and the ocean model has 19 vertical levels. The terrestrial carbon model is a modified version of the MOSES2 land surface model and the TRIFFID dynamic vegetation model (Meissner et al. 2003; Matthews et al. 2004, 2005a). MOSES2 calculates carbon fluxes for soil and five PFTs. Net primary production is a function of CO_2, light, soil moisture, temperature, nutrients, and autotrophic respiration. Photosynthesis is calculated using a leaf-level model for C_3 and C_4 plants. Aggregated carbon fluxes are passed to TRIFFID, which updates the fraction of each PFT based on Lotka–Volterra competition equations. Carbon is passed to the soil through litterfall and vegetation mortality. Soil carbon is in a single pool and decomposition is controlled by soil temperature and water stress using a Q10 formulation (Q10 = 2.). Only inorganic ocean carbon is included, based on the OCMIP abiotic protocol. The ice-sheet and ocean biology models are not used. Isopycnal mixing and flux corrected transport were used in the ocean model and the sea ice model is a simple, single layer, thermodynamic version, with elastic–viscous–plastic dynamics. Water, energy, and carbon are conserved with no flux adjustments.

CLIMBER2-Lund–Potsdam–Jena (LPJ) is a coupled climate–carbon cycle model (Sitch et al. 2005). CLIMBER-2 (Petoukhov et al. 2000) comprises a 2.5-dimensional dynamical–statistical atmosphere model with a coarse spatial resolution of $10°$ latitude and $51°$ longitude, a three-basin, zonally averaged ocean model, a sea ice model with latitudinal resolution of $2.5°$. The LPJ dynamic global vegetation model (Sitch et al. 2003) incorporates a coupled photosynthesis–water balance scheme, plant resource competition, population dynamics, fire disturbance, and soil biogeochemistry. The decomposition model includes above- and below-ground

litter pools as well as intermediate and slow soil organic matter pools. Decomposition is soil temperature and moisture dependent; temperature dependence follows the modified Q10 approach. In coupled simulations, LPJ is run on a 0.5° spatial resolution and is driven by monthly anomalies of surface air temperature, precipitation, and cloudiness, computed in CLIMBER-2 and added to the background climate patterns from the Climate Research Unit (CRU) climate dataset (New et al. 1999, 2000). The oceanic carbon cycle includes standard inorganic biogeochemistry (Brovkin et al. 2002) and the marine biota NPZD model by Six and Maier-Reimer (1996) with PO_4 as the limiting nutrient.

The climate module of the Bern Carbon Cycle-Climate (Bern CC) model (Joos et al. 2001) is an impulse response–empirical orthogonal function (IRF–EOF) substitute driven by radiative forcing. An IRF for surface-to-deep mixing of heat characterize the adjustment time of the climate system to changes in radiative forcing, whereas EOFs describe the spatial patterns of perturbations in surface temperature, precipitation, and cloud cover on a grid of $2.5° × 3.75°$. The equilibrium climate sensitivity is set here to 2.5°C. The terrestrial carbon model [the LPJ Dynamic Global Vegetation Model (DGVM); Sitch et al. 2003] simulates photosynthesis, respiration, fire, and the growth and competition of nine PFTs. Photosynthesis is based on a simplified Farquhar scheme, with leaf-level optimized nitrogen allocation and an empirical convective boundary layer parameterization to couple the carbon and water cycle. For each PFT, carbon is stored in four vegetation and three litter pools. Two soil organic matter pools receive input from all litter pools on each grid cell. Decomposition of soil and litter organic carbon is dependent on soil temperature by a modified Arrhenius relationship and on soil moisture. The High Latitude Exchange/Interior Diffusion–Advection Model (HILDA) box-diffusion type ocean model (Joos et al. 1996) simulates surface-to-deep exchange of carbon and heat, taking into account the effect of warming on carbon chemistry. Marine biological processes and potential circulation changes are not modeled.

3. Results

a. Simulated atmospheric CO_2

In the coupled simulations, atmospheric CO_2 concentration ranges between 730 ppm for LLNL and 1020 ppm for HadCM3LC by 2100 (Fig. 1a). Apart from UMD and CSM-1, all models simulate historical CO_2 close to that observed. The atmospheric CO_2 concentrations in the CSM-1 simulation during the twentieth century are low because of the simulation neglected

historical land-use emissions, but would reach the observed value if the modeled airborne fraction was used to scale the emissions. UMD atmospheric CO_2 is too high because it has a relatively weak CO_2 fertilization effect. The partitioning between contemporary land versus oceanic uptake is generally in good agreement with atmospheric-based estimates (Prentice et al. 2001; LeQuéré et al. 2003). However UMD, HadCM3LC, CSM-1, and FRCGC simulate lower than the observed land uptakes for the 1980s and 1990s, whereas LLNL simulates a larger value than the observation derived land uptake estimates. Some care is required, however, interpreting these findings because terrestrial carbon uptake in the models is driven primarily by CO_2 fertilization while many data-based studies (e.g., Schimel et al. 2001) highlight other mechanisms such as recovery from past land-use change. Also, historical carbon flux anomalies such as the one following the Mount Pinatubo eruption are not represented in these coupled models.

Differences in the behavior of the different coupled models regarding the simulated atmospheric CO_2 growth rate become important around 2025. When comparing the coupled and uncoupled simulated atmospheric CO_2, all models show a larger CO_2 in the coupled simulation (Fig. 1b). That is to say, all models have a positive climate–carbon cycle feedback. This confirms the initial findings of Cox et al. (2000) and Friedlingstein et al. (2001). However, the additional CO_2 concentration induced by this feedback ranges between 20 ppm for CSM-1 and 200 ppm for HadCM3LC. Six of the 11 models have a CO_2 concentration difference ranging between 50 and 100 ppm. There is no systematic difference between the behaviors of OAGCMs and EMICs.

b. Carbon budget changes

As noted above for the model results for the historical period, the coupled models exhibit large differences in the land and ocean partitioning of carbon fluxes in the twenty-first century. The 2100 land net CO_2 flux ranges between an uptake of 11GtC yr^{-1} for LLNL to a source of 6GtC yr^{-1} for HadCM3LC (Fig. 1c). The range of the ocean carbon fluxes is much smaller. The lowest uptake is simulated by LLNL and reaches 3.8 GtC yr^{-1} by 2100; the largest is simulated by UMD and reaches 10 GtC yr^{-1} (Fig. 1e). There is some compensation between land and ocean fluxes through the atmospheric CO_2. For example, LLNL has the largest land uptake and the lowest ocean uptake; UMD has the largest ocean uptake and the second lowest land uptake. We note that only two models (HadCM3LC and
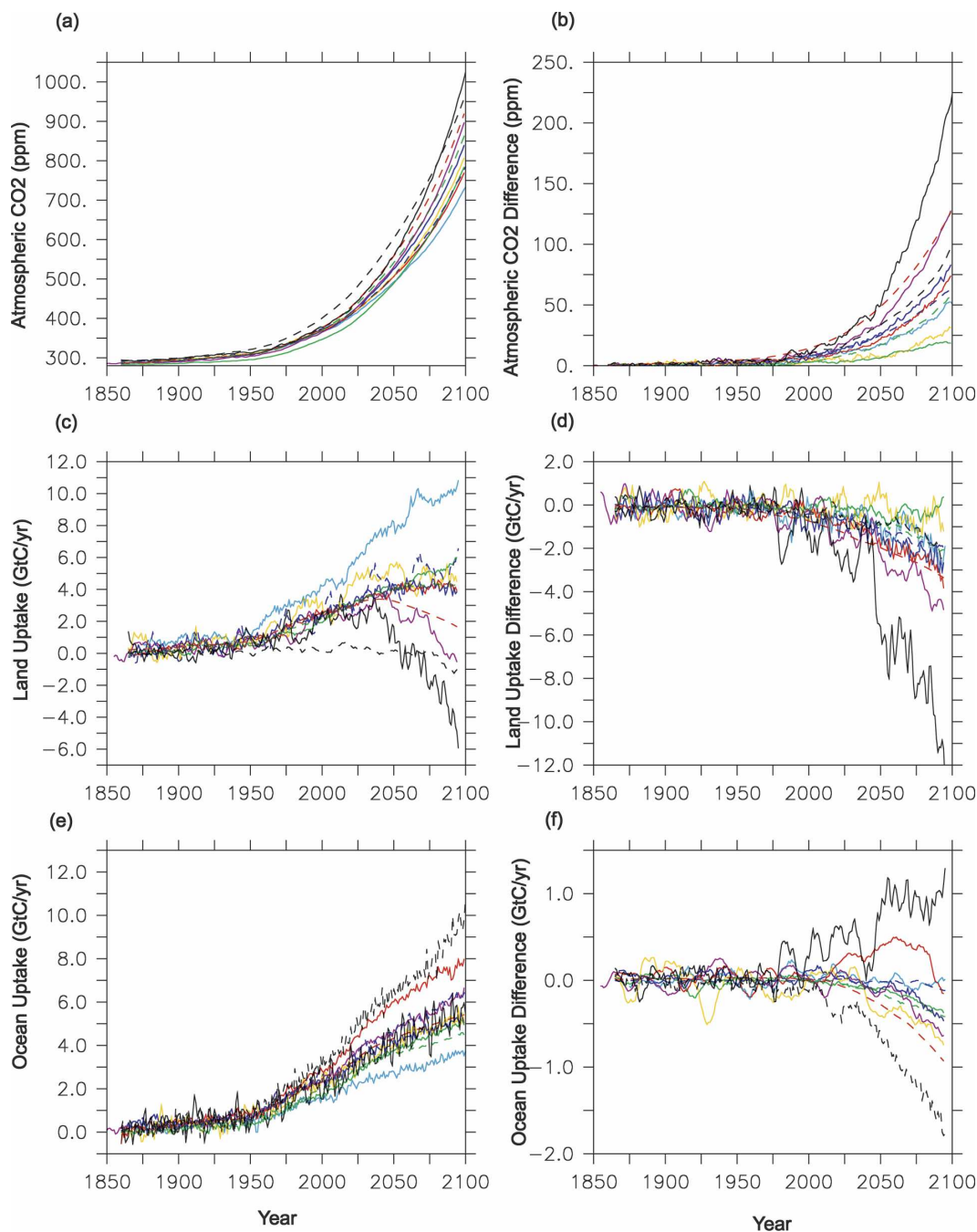
FIG. 1. (a) Atmospheric CO_2 for the coupled simulations (ppm) as simulated by the HadCM3LC (solid black), IPSL-CM2C (solid red), IPSL-CM4-LOOP (solid yellow), CSM-1 (solid green), MPI (solid dark blue), LLNL (solid light blue), FRCGC (solid purple), UMD (dash black), UVic-2.7 (dash red), CLIMBER (dash green), and BERN-CC (dash blue). (b) Atmospheric CO_2 difference between the coupled and uncoupled simulations (ppm). (c) Land carbon fluxes for the coupled runs (GtC yr^{-1}). (d) Differences between coupled and uncoupled land carbon fluxes (GtC yr^{-1}). (e), (f) Same as (c), (d), respectively, for the ocean carbon fluxes.

UMD) simulate a sink/source transition for the land carbon flux. The source arising in the UMD simulation is mainly due to the fact that this model already simulates a very weak land carbon uptake in the uncoupled simulation (uptake of 0.3 GtC yr^{-1} for the 1990s and 1 GtC yr^{-1} by 2100). These two models are also the ones that simulate the larger atmospheric CO_2 concentration by 2100, as the land is a source of CO_2 at that time. This

TABLE 2. Simulated air, land, and ocean-borne fractions in 2100 of the cumulative anthropogenic CO_2 emissions over the entire period of the coupled (and uncoupled) model runs.

	Airborne fraction	Land-borne fraction	Ocean-borne fraction
HadCM3LC	0.71 (0.49)	0.05 (0.31)	0.24 (0.20)
IPSL-CM2C	0.47 (0.40)	0.22 (0.30)	0.32 (0.30)
IPSL-CM4-LOOP	0.50 (0.48)	0.27 (0.28)	0.23 (0.24)
CSM1	0.53 (0.52)	0.25 (0.26)	0.21 (0.22)
MPI	0.53 (0.45)	0.22 (0.30)	0.24 (0.24)
LLNL	0.42 (0.38)	0.45 (0.50)	0.15 (0.16)
FRCGC	0.62 (0.49)	0.14 (0.27)	0.27 (0.28)
UMD	0.66 (0.56)	0.01 (0.06)	0.36 (0.40)
UVic-2.7	0.60 (0.48)	0.18 (0.28)	0.23 (0.25)
CLIMBER	0.57 (0.51)	0.22 (0.27)	0.20 (0.21)
BERN-CC	0.48 (0.42)	0.26 (0.32)	0.26 (0.26)

shows that the ocean compensation is limited within these time scales.

The difference between the coupled and uncoupled land and ocean carbon fluxes is shown in Figs. 1d,f, respectively. All models produce a negative anomaly for the atmosphere–land fluxes, although this anomaly is weak for CSM-1 and IPSL-CM4-LOOP. The difference between the atmosphere–land fluxes of the coupled and uncoupled runs ranges between less than 1GtC yr^{-1} (CSM-1) and more than 10GtC yr^{-1} (for HadCM3LC) by 2100. The range of the changes in ocean uptake is much lower than on the land side. It ranges between a reduction of 2GtC yr^{-1} (UMD) to an increase of about 1GtC yr^{-1} in HadCM3LC. The increase in ocean uptake is mainly due to the land–ocean compensation mentioned above. This is the ocean response to the additional atmospheric CO_2 resulting from the terrestrial carbon release, as shown before by Dufresne et al. (2002). Indeed, all models show negative sensitivity of ocean uptake to climate change alone (see section 4).

Table 2 shows the fraction of the cumulative anthropogenic CO_2 emissions that reside in each reservoir at the end of the simulation, 2100, for both the coupled and uncoupled simulations from each model. For all models, the airborne fraction of the coupled simulation is always larger than the one of the uncoupled simulation, as a result of the reduction in land carbon uptake.

4. Feedback analysis

The effect of climate-induced changes in carbon budget on the rate of increase of atmospheric CO_2 can be quantified by

$$\Delta C_A^c = 1/(1 - g) \, \Delta C_A^u, \tag{1}$$

where ΔC_A^c is the change in atmospheric CO_2 in the coupled run, ΔC_A^u is the corresponding change in CO_2 in the uncoupled run, and g is the gain of the climate–carbon feedback as defined for climate system feedbacks (Hansen et al. 1984). To isolate the key influential components, the model experiments are compared in terms of the response of the land and ocean carbon uptake to climate and CO_2 (Friedlingstein et al. 2003). One can define the change in land and ocean carbon storage as

$$\Delta C_L^c = \beta_L \Delta C_A^c + \gamma_L \Delta T^c, \tag{2}$$

$$\Delta C_O^c = \beta_O \Delta C_A^c + \gamma_O \Delta T^c, \tag{3}$$

where ΔC_L^c and ΔC_O^c are the change in land and ocean carbon storage (in GtC) in the coupled simulation arising from an increase in atmospheric CO_2 concentration of ΔC_A^c (ppm) and a temperature increase of ΔT^c (K). Here β_L (β_O) is the land (ocean) carbon sensitivity to atmospheric CO_2, and γ_L (γ_O) is the land (ocean) carbon sensitivity to climate change.

Similarly, one can define the same storage changes for the uncoupled simulation as

$$\Delta C_L^u = \beta_L \Delta C_A^u, \tag{4}$$

$$\Delta C_O^u = \beta_O \Delta C_A^u. \tag{5}$$

The effect of changing CO_2 on global mean temperature can be approximated as

$$\Delta T^c = \alpha \Delta C_A^c, \tag{6}$$

where α is the linear transient climate sensitivity to CO_2 in K ppm^{-1}. Equations (1), (2), (3), and (6) can be manipulated to yield an expression for the gain in terms

of the sensitivity coefficients of the land and ocean carbon cycle (Friedlingstein et al. 2003):

$$g = -\alpha(\gamma_L + \gamma_O)/(1 + \beta_L + \beta_O). \quad (7)$$

Note that the gain of the carbon cycle is larger for higher effective climate sensitivities (Friedlingstein et al. 2003; Jones et al. 2003a; Govindasamy et al. 2005; Matthews et al. 2005a,b) and for more negative values of γ_L and γ_O. Conversely, the climate–carbon cycle feedback is weaker if ocean and land uptake respond very positively to increasing CO_2 (i.e., large β_L and β_O; Friedlingstein et al. 2003). We understand that this analysis neglects some of the nonlinear aspects of the climate–carbon cycle feedback; however, it provides a valuable starting point for characterizing the different model responses. Also we use temperature change as a proxy for climate change in this analysis, but the changes in carbon fluxes we use here were simulated by the coupled models and result obviously from changes in the full climate system (hydrology, radiation, oceanic circulation, etc.) Also, note that here we apply a transient feedback analysis, while equilibrium feedback values would be quite different from the transient ones.

a. Climate response to atmospheric CO_2

The scope of this paper is not to analyze the climate sensitivity of the different coupled models; this is being done extensively elsewhere (e.g., Houghton et al. 2001; Murphy et al. 2004; Petoukhov et al. 2005). Figure 2a shows the transient temperature increase of the 11 C^4MIP coupled models as a function of atmospheric CO_2. The climate sensitivity α is defined here from Eq. (6) as the ratio of global temperature change to atmospheric CO_2 change in the coupled simulation. CSM-1 has the lowest climate sensitivity (about 1 K at the time of $2 \times CO_2$, i.e., 560 ppm); MPI, IPSL-CM4-LOOP, and HadCM3LC have the highest climate sensitivity (2.5 K at the time of $2 \times CO_2$). A factor of 2 in α will directly translate into at least a factor of 2 in g, the climate–carbon gain. This highlights the importance of reducing the uncertainty in climate sensitivity.

b. Increase in land carbon uptake with atmospheric CO_2

Although the experimental evidence of CO_2 fertilization at the patch scale is equivocal (e.g., Nowak et al. 2004), most climate–carbon cycle models reproduce the current land–carbon sink by this mechanism. Figure 2c shows the change in land carbon storage from each of the uncoupled C^4MIP runs against atmospheric CO_2 concentration for uncoupled simulations (i.e., no climate feedback). There is a large variability amongst

models for the land response to CO_2. At the time of $2 \times CO_2$, the accumulated land uptake ranges from less than 100 GtC (UMD) to almost 800 GtC (LLNL). The derived values of β_L hence range from 0.2 (UMD) to 2.8 GtC ppm^{-1} (LLNL). However, 9 of the 11 models occupy the range 0.9–1.6. It is clear from Eq. (7) that a large β_L would reduce the magnitude of the carbon cycle feedback. In a sensitivity experiments with the LLNL model, in which the CO_2-fertilization effect was capped at current day, Thompson et al. (2004) showed that the climate–carbon feedback almost doubles when CO_2 fertilization saturates by the year 2000.

This large range in carbon uptake sensitivity to atmospheric CO_2 arises from the model NPP response to CO_2. UMD is the only model with a very low β_L and is indeed the one having almost no sensitivity of NPP to atmospheric CO_2. By contrast, LLNL shows the largest NPP response to CO_2, with NPP increasing by 60% at the time of $2 \times CO_2$. However, apart from these three outliers, the majority of the models have a very similar NPP sensitivity to CO_2. We note that none of the models account for an explicit treatment of the nitrogen cycle. The differences seen here are not due to inclusion versus omission of nitrogen limitations.

c. Increase in ocean carbon uptake with atmospheric CO_2

The ocean will take up CO_2 at a rate that depends on the difference between the partial pressures of CO_2 in the atmosphere and the surface ocean. Model estimates of uptake differ primarily because of differences in the rate at which carbon is transported from the surface ocean to depth by the ocean circulation (e.g., thermocline ventilation, deep and intermediate water formation). We estimate the ocean carbon model sensitivity to atmospheric CO_2 increase (β_O) from the uncoupled simulations. At the time of $2 \times CO_2$, there is a factor of 2 in the accumulated oceanic carbon uptake. It ranges from about 250 GtC (HadCM3LC, LLNL, and Climber) to 500 GtC (IPSL-CM2C; Fig. 2d). The coefficient β_O (defined here as the slope of the line in Fig. 2d by 2100) ranges from 0.8 to 1.6 GtC ppm^{-1}.

d. Dependence of land carbon storage on climate

Land carbon storage depends on the balance between the input of carbon as NPP, and the loss of carbon as heterotrophic respiration (R_h). Both of these terms are strongly climate dependent. Plant productivity depends on water availability and ambient temperature. Changes in water availability depend critically upon uncertain regional aspects of climate change projections and are therefore likely to be a dominant source of uncertainty.
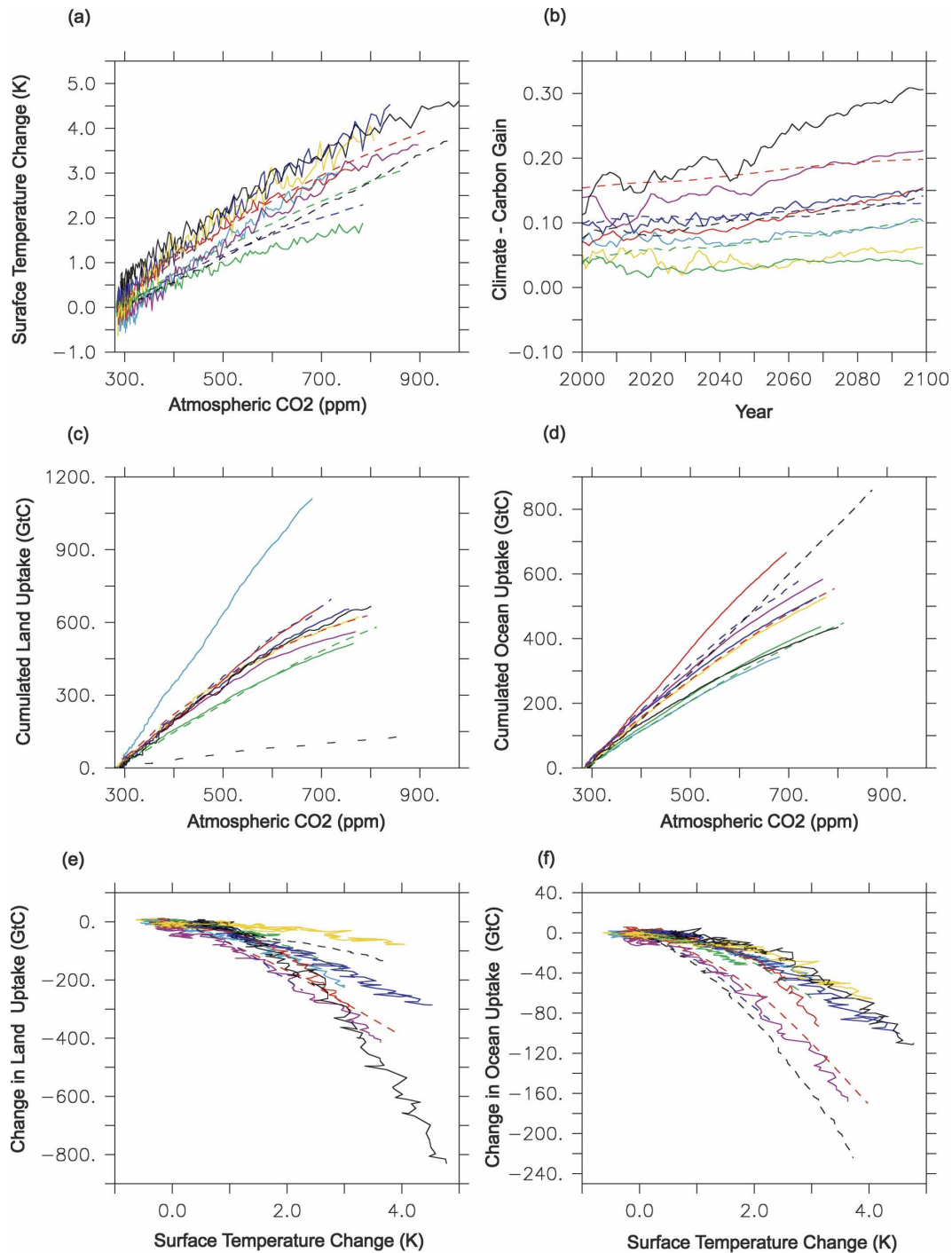
FIG. 2. (a) Simulated surface temperature response to atmospheric CO_2. (b) Time evolution of the climate–carbon gain. (c) Sensitivity of land carbon storage to atmospheric CO_2 (uncoupled runs). (d) Same as (c) for the ocean. (e) Sensitivity of land carbon storage to climate (coupled runs). (f) Same as (e) for the ocean. Color code is the same as in Fig. 1.

The specific rate of heterotrophic respiration (i.e., the respiration rate per unit respiring carbon) is typically assumed to increase with temperature, consistent with a long history of laboratory and field measure-ments, although there is an ongoing debate about the extent of acclimation of R_h to higher temperatures (Giardini and Ryan 2000; Luo et al. 2001; Knorr et al. 2005). The C^{4}MIP models utilize different representa-
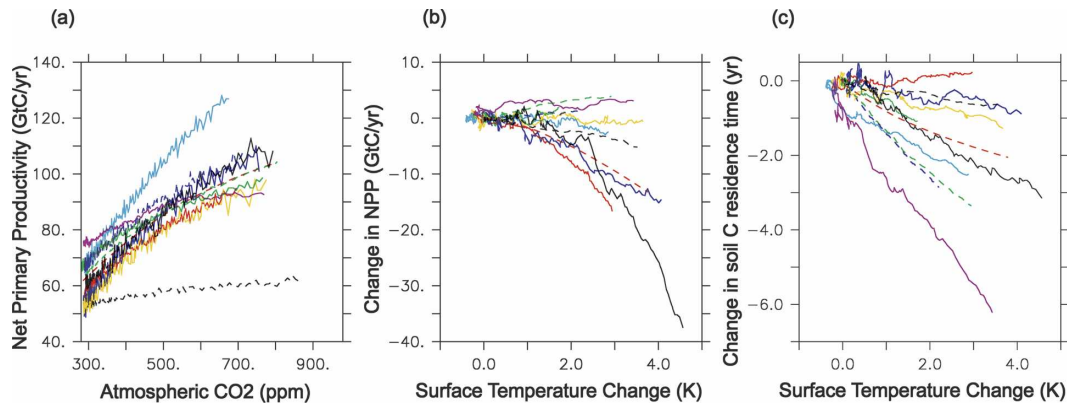
FIG. 3. (a) Simulated NPP sensitivity to atmospheric CO_2 (uncoupled run). (b) Simulated NPP sensitivity to climate (coupled run − uncoupled run). (c) Simulated soil carbon turnover time sensitivity to climate (coupled run − uncoupled run). Color code is the same as in Fig. 1.

tions of soil carbon turnover, ranging from single-pool models (HadCM3LC) to nine-pool models (CSM-1). However, all of the models assume an acceleration of decay with temperature. This is often characterized through the parameter Q10, the increase of the specific respiration rate for every 10-K increase in surface (or soil) temperature. Q10 is set to 2 for most models, however MPI has a Q10 of 1.5, and UMD has Q10 ranging from 1.1 for the slow soil carbon pool to 2.2 for the fast turnover soil carbon pool.

The overall sensitivity of land carbon storage to climate is quantified in terms of γ_L. The difference in carbon uptake between the coupled and the uncoupled simulations is the combination of different climate, but also different atmospheric CO_2 [Eqs. (2) and (4)]. We isolate the "climate alone" impact on land carbon uptake as $\Delta C_L^{clim} = (\Delta C_L^c - \Delta C_L^u) - \beta_L (\Delta C_A^c - \Delta C_A^u)$, where the first term is the change in land carbon uptake between the coupled and uncoupled run [Eqs. (2) minus (4)], and the second term accounts for the difference in atmospheric CO_2 between the coupled and the uncoupled runs. The γ factor for the land is then defined as: $\gamma_L = \Delta C_L^{clim}/\Delta T^c$. Figure 2e shows ΔC_L^{clim} as a function of ΔT^c for each model. Although this change in land carbon storage is negative for all models, it ranges from less than 100 GtC (CSM-1 and IPSL-CM4-LOOP) to about 800 GtC for a 4°C warming in the HadCM3LC simulation ($\gamma_L = -177$ GtC K^{-1}). However, seven of the eleven models lie in the range −40 to −105 GtC K^{-1}. The strong negative impact of climate change on land carbon storage in the HadCM3LC model is the primary reason for its large positive climate–carbon cycle feedback (Friedlingstein et al. 2003). Also, this reduction of NEP with climate change occurs at all latitudes for HadCM3LC, whereas other models show compensation between NEP reduction in the

Tropics and NEP increase in the mid- or high latitudes. A number of studies have considered this higher than the average sensitivity of HadCM3LC, including the marked drying under climate change in the Amazon basin (Cox et al. 2004), the choice of Q10 = 2 for soil respiration (Jones et al. 2003b), the use of a single-pool soil carbon model (Jones et al. 2004), and the parameterization of plant respiration (Huntingford et al. 2004). In each case the characteristics of the Hadley Centre model appear to encourage a larger γ_L, but no single assumption accounts completely for the large sensitivity.

Since carbon uptake is the difference between NPP and heterotrophic respiration, we separately analyze the response of these two terms to climate. Similarly to the correction for NEP described above, we correct the changes in NPP in order to isolate the impact of climate change. It is clear from Fig. 3b that there is no model consensus on the global NPP response to climate change. Two models (FRCGC and CLIMBER) simulate an increase in NPP, five models simulate very little change (less than 10% of initial NPP), and four models (MPI, UVic-2.7, IPSL-CM2C, and HadCM3LC) show large decrease of NPP with climate (as large as 6 GtC °C^{-1} for HadCM3LC). A recent sensitivity study by Matthews et al. (2005b) using the UVic-2.7 model found that the carbon cycle–climate feedback is indeed highly sensitive to the response of NPP to climate changes, suggesting that part of the range of feedbacks among the models represented here can be attributed to the range of NPP response to climate change.

It is important to point out that these are the global sensitivities, and they may reflect a large variability at the regional level that is hidden here. Indeed, there is a fairly good agreement across the models in the high latitudes where almost all models simulate a climate-

TABLE 3. Carbon cycle gain, g, along with component sensitivities of climate to CO_2 (α), land and ocean carbon storage to CO_2 (β_L, β_O), and land and ocean carbon storage to climate (γ_L, γ_O). Calculations are done for year 2100.

Models	α (K ppm^{-1})	β_L (GtC ppm^{-1})	β_O (GtC ppm^{-1})	γ_L (GtC K^{-1})	γ_O (GtC K^{-1})	Gain
HadCM3LC	0.0066	1.3	0.8	−177	−24	0.31
IPSL-CM2C	0.0065	1.6	1.6	−98	−30	0.15
IPSL-CM4-LOOP	0.0072	1.3	1.1	−20	−16	0.06
CSM-1	0.0038	1.1	0.9	−23	−17	0.04
MPI	0.0082	1.4	1.1	−65	−22	0.20
LLNL	0.0068	2.8	0.9	−70	−14	0.10
FRCGC	0.0059	1.2	1.2	−112	−46	0.21
UMD	0.0056	0.2	1.5	−40	−67	0.14
UVic-2.7	0.0063	1.2	1.1	−98	−43	0.20
CLIMBER	0.0053	1.1	0.9	−57	−22	0.10
BERN-CC	0.0046	1.6	1.3	−105	−39	0.13
Models avg	0.0061	1.35	1.13	−79	−30	0.15

induced increase of NPP and NEP. The response of tropical NPP and NEP shows more variability across models, although the majority of the models simulate a decrease of NPP and NEP in these regions. A possible explanation is that high-latitude NPP is more temperature dependent (in terms of duration of snow cover and growing season length) whereas tropical NPP may be more moisture dependent and therefore have greater spread both regionally and between models because the hydrological cycle is more difficult to simulate. Also, there is no clear difference in term of γ_L between the dynamic vegetation models and the static vegetation models.

To analyze the respiration response to climate, we first estimated the mean turnover time of dead carbon (litter plus soil carbon pools, τ_{LS}) in the models as the ratio of total dead carbon to heterotrophic respiration. The change in τ_{LS} as a function of temperature between the coupled and the uncoupled simulations is shown in Fig. 3c. All but one model simulated a reduction of soil carbon turnover time, that is to say an increase in specific respiration with climate. However, there is a large discrepancy among the models. IPSL-CM2C shows no sensitivity of global turnover time to climate, whereas Climber, LLNL, and HadCM3LC show a large negative impact of climate on τ_{LS} (up to -1 yr $°C^{-1}$). The peculiar response of IPSL-CM2C comes from the positive sensitivity of turnover time to soil water content, which coincidently counterbalances its negative sensitivity to temperature.

e. Dependence of ocean carbon uptake on climate

Climate change can affect ocean carbon uptake by influencing the transport of carbon to depth by both the large-scale circulation (e.g., by slowing down the thermohaline circulation) and the biological pump. In par-

ticular, increases in thermal and freshwater stratification as the sea surface warms may suppress vertical transport. As for the land, we calculate the climate impact on ocean carbon uptake as $\Delta C_O^{clim} = (\Delta C_O^c - \Delta C_O^u) - \beta_O (\Delta C_A^c - \Delta C_A^u)$; the γ factor for the ocean is defined as $\gamma_O = \Delta C_O^{clim} / \Delta T^c$. Figure 2f shows ΔC_O^{clim} as a function of the simulated temperature change (ΔT^c) for all models. Here there is a clear difference between the EMICs behavior and the tridimensional OGCMs. The EMICS tend to simulate a much larger negative γ_O than the OGCMS. Two of the EMICs employ zonally averaged ocean models (CLIMBER, BERN) and one uses only simple slab mixed layer ocean model with specified present-day ocean heat transports (UMD). These ocean components may not be adequate to capture the two-dimensional ocean carbon uptake field and its climate sensitivity. The fourth EMIC (UVic-2.7), on the other hand, incorporates a full OGCM but has no representation of ocean biology, perhaps explaining some of the differences from the comprehensive coupled OAGCMs. The coupled OAGCMs show a greater degree of agreement for values of γ_O (at the exception of FRCGC). A 1°C global surface temperature warming leads to an ocean uptake reduction of about 20 GtC. Note that this is a transient sensitivity, while equilibrium sensitivity of atmospheric CO_2 to ocean temperature increase is much higher (see Archer et al. 2004). Also, as for the land, we note the nonlinearity in the response, that is, a larger warming inducing a larger sensitivity.

5. Discussion and conclusions

Table 3 summarizes the α, β, and γ coefficients and the climate–carbon cycle gain from each of the C[4]MIP models. All models have a positive gain factor, g, that is

to say, climate change will increase the fraction of anthropogenic CO_2 emissions that remain airborne, producing a positive feedback on climate change. For two models (CSM-1 and IPSL-CM4-LOOP), however, this gain is very small. We also note that the gain is not constant in time (Fig. 2b). There is a clear tendency across the models to show an increase in g with time. This amplification of the gain has to be found in the evolution of γ_L, and γ_O, both increasing with time. By 2100, the additional CO_2 ranges between 20 and 200 ppm. By design, the C^4MIP simulations cannot directly estimate the additional warming associated with this higher CO_2 level; the climate of the uncoupled simulation being held at preindustrial CO_2 level. However, knowing α, the models' climate sensitivity from the coupled simulations, we can estimate the warming that would occur if the climate model was forced by the atmospheric CO_2 of the uncoupled simulation (assuming the same climate sensitivity). The additional warming, due to the climate–carbon cycle feedback can hence be estimated as

$$\Delta T^c - \Delta T^u = \alpha(\Delta C_A^c - \Delta C_A^u).$$

This leads to an additional warming ranging between $0.1°$ and $1.5°C$.

In summary, CO_2 increase alone will tend to enhance carbon storage by both the land and the ocean, whereas climate change alone will tend to release land and ocean carbon to the atmosphere. Together, ocean and land still will act as a sink for anthropogenic carbon during the whole twenty-first century, but the relative importance of these removal mechanisms is reduced because of carbon–climate feedbacks as the airborne fraction of anthropogenic emission increases for all coupled models relative to their uncoupled simulations (Table 2). However, there is much less agreement on the magnitude of these various effects. All but one model (HadCM3LC) produce a positive climate–carbon cycle gain in the range 0. to 0.2. Also, among the nine models producing a gain larger than 0.1, all but one (UMD) attribute this gain to the land (γ_L lower than γ_O).

To reduce the large uncertainties in climate–carbon cycle projections, it is critically important that carbon cycle models are more completely constrained by observational data (e.g., HadCM3LC simulations of the twentieth-century land carbon cycle have been performed, forced by observed SSTs; Jones and Warnier 2004). To do this the models need to be more complete so that they are more obviously comparable to the real world. In the case of the land carbon cycle, current limitations include the lack of consistent modeling of the effects of land-use change and regrowth (Sitch et al. 2005) and the neglect of carbon–nutrients interactions. For the ocean carbon cycle, there is a need for more complete treatments of ocean ecosystems (e.g., resolving more than one phytoplankton functional type), micronutrient limitation (e.g., Fe), and ocean acidification impacts on the calcium carbonate cycle. The first generation C^4MIP runs may be helpful in prioritizing the modeling and experimental work in each of these areas.

REFERENCES

Archer, D., P. Martin, B. Buffett, V. Brovkin, S. Rahmstorf, and A. Ganopolski, 2004: The importance of ocean temperature to global biogeochemistry. *Frontiers Earth Planet. Sci. Lett.,* **222,** 333–348.

Aumont, O., J. C. Orr, P. Monfray, G. Madec, and E. Maier-Reimer, 1999: Nutrient trapping in the equatorial Pacific: The ocean circulation solution. *Global Biogeochem. Cycles,* **13,** 351–371.

——, E. Maier-Reimer, S. Blain, and P. Monfray, 2003: An ecosystem model of the global ocean including Fe, Si, P co-limitations. *Global Biogeochem. Cycles,* **17,** 1060, doi:10.1029/2001GB00174.

Ball, J. T., I. E. Woodrow, and J. A. Berry, 1986: A model predicting stomatal conductance and its contribution to the control of photosynthesis under different environmental conditions. *Progress in Photosynthesis Research*, J. Biggins, Ed., Vol. 4, Martin Nijhoff, 221–224.

Berthelot, M., P. Friedlingstein, P. Ciais, J.-L. Dufresne, and P. Monfray, 2005: How uncertainties in future climate change predictions translate into future terrestrial carbon fluxes. *Global Change Biol.,* **11,** 959–970.

Bonan, G. B., 1996: The NCAR Land Surface Model (LSM version 1.0) coupled to the NCAR Community Climate Model. NCAR Tech. Note NCAR/TN-429+STR, 171 pp.

Bousquet, P., P. Peylin, P. Ciais, C. Le Quéré, P. Friedlingstein, and P. P. Tans, 2000: Regional changes in carbon dioxide fluxes of land and oceans since 1980. *Science,* **290,** 1342–1346.

Boville, B. A., and P. R. Gent, 1998: The NCAR climate system model, version one. *J. Climate,* **11,** 1115–1130.

——, J. T. Kiehl, P. J. Rasch, and F. O. Bryan, 2001: Improvements to the NCAR CSM-1 for transient climate simulations. *J. Climate,* **14,** 164–179.

Brovkin, V., J. Bendtsen, M. Claussen, A. Ganopolski, C. Kubatzki, V. Petoukhov, and A. Andreev, 2002: Carbon cycle,

vegetation and climate dynamics in the Holocene: Experiments with the CLIMBER-2 model. *Global Biogeochem. Cycles,* **16,** 1139, doi:10.1029/2001GB001662.

——, S. Sitch, W. von Bloh, M. Claussen, E. Bauer, and W. Cramer, 2004: Role of land cover changes for atmospheric CO_2 increase and climate change during the last 150 years. *Global Change Biol.,* **10,** 1253–1266.

Chuck, A., T. Tyrrell, I. J. Totterdell, and P. M. Holligan, 2005: The oceanic response to carbon emissions over the next century: Investigation using three ocean carbon cycle models. *Tellus,* **57B,** 70–86.

Collatz, G. J., J. T. Ball, C. Grivet, and J. A. Berry, 1991: Physiological and environmental regulation of stomatal conductance, photosynthesis, and transpiration: A model that includes a laminar boundary layer. *Agric. For. Meteor.,* **53,** 107–136.

——, M. Ribas-Carbo, and J. A. Berry, 1992: Coupled photosynthesis-stomatal conductance model for leaves of C4 plants. *Aust. J. Plant Physiol.,* **19,** 519–538.

Cox, P. M., 2001: Description of the TRIFFID dynamic global vegetation model. Tech. Note 24, Hadley Centre, Met Office, 16 pp.

——, R. A. Betts, C. B. Bunton, R. L. H. Essery, P. R. Rowntree, and J. Smith, 1999: The impact of new land surface physics on the GCM simulation of climate and climate sensitivity. *Climate Dyn.,* **15,** 183–203.

——, ——, C. D. Jones, S. A. Spall, and I. J. Totterdell, 2000: Acceleration of global warming due to carbon-cycle feedbacks in a coupled climate model. *Nature,* **408,** 184–187.

——, P. Friedlingstein, and P. Rayner, 2002: Modelling climate–carbon cycle feedbacks: A cross disciplinary collaboration priority. *IGBP Global Change Newslet.,* **49,** 12–14.

——, R. A. Betts, M. Collins, P. P. Harris, C. Huntingford, and C. D. Jones, 2004: Amazonian forest dieback under climate-carbon cycle projections for the 21st century. *Theor. Appl. Climatol.,* **78,** 137–156.

Cramer, W., and Coauthors, 2001: Global response of terrestrial ecosystem structure and function to CO_2 and climate change: Results from six dynamic global vegetation models. *Global Change Biol.,* **7,** 357–373.

Dickinson, R. E., M. Shaikh, B. Ross, and L. Graumlich, 1998: Interactive canopies for a climate model. *J. Climate,* **11,** 2823–2836.

Doney, S. C., K. Lindsay, and J. K. Moore, 2003: Global ocean carbon cycle modeling. *Ocean Biogeochemistry: The Role of the Ocean Carbon Cycle in Global Change,* M. J. R. Fasham, Ed., Springer-Verlag, 217–238.

——, ——, I. Fung, and J. John, 2006: Natural variability in a stable, 1000-yr global coupled climate–carbon cycle simulation. *J. Climate,* **19,** 3033–3054.

Dufresne, J.-L., J. Quass, O. Boucher, S. Denvil, and L. Fairhead, 2005: Contrasts in the effects on climate of anthropogenic sulfate aerosols between the 20th and 21st century. *Geophys. Res. Lett.,* **32,** L21703, doi:10.1029/2005GL023619.

Farquhar, G. D., S. von Caemmerer, and J. A. Berry, 1980: A biogeochemical model of photosynthesis in leaves of C3 species. *Planta,* **149,** 78–90.

Field, C. B., J. T. Randerson, and C. M. Malmström, 1995: Global net primary production: Combining ecology and remote sensing. *Remote Sens. Environ.,* **51,** 74–88.

Foley, J. A., I. C. Prentice, N. Ramankutty, S. Levis, D. Pollard, S. Sitch, and A. Haxeltine, 1996: An integrated biosphere model of land surface processes, terrestrial carbon balance and vegetation dynamics. *Global Biogeochem. Cycles,* **10,** 603–628.

Friedlingstein, P., I. Fung, E. Holland, J. John, G. Brasseur, D. Erickson, and D. Schimel, 1995: On the contribution of CO_2 fertilization to the missing biospheric sink. *Global Biogeochem. Cycles,* **9,** 541–556.

——, G. Joel, C. B. Field, and I. Y. Fung, 1999: Toward an allocation scheme for global terrestrial carbon models. *Global Change Biol.,* **5,** 755–770.

——, L. Bopp, P. Ciais, J.-L. Dufresne, L. Fairhead, H. LeTreut, P. Monfray, and J. Orr, 2001: Positive feedback between future climate change and the carbon cycle. *Geophys. Res. Lett.,* **28,** 1543–1546.

——, J.-L. Dufresne, P. M. Cox, and P. Rayner, 2003: How positive is the feedback between climate change and the carbon cycle? *Tellus,* **55B,** 692–700.

Fung, I., P. Rayner, and P. Friedlingstein, 2000: Full-form earth system models: Coupled carbon-climate interaction experiment (the flying leap). *IGBP Global Change Newslet.,* **41,** 7–8.

——, S. C. Doney, K. Lindsay, and J. John, 2005: Evolution of carbon sinks in a changing climate. *Proc. Natl. Acad. Sci. USA,* **102,** 11 201–11 206.

Gerber, S., F. Joos, P. P. Brügger, T. F. Stocker, M. E. Mann, S. Sitch, and M. Scholze, 2003: Constraining temperature variations over the last millennium by comparing simulated and observed atmospheric CO_2. *Climate Dyn.,* **20,** 281–299.

Giardina, C., and M. Ryan, 2000: Evidences that decomposition rates of organic carbon in mineral soil do not vary with temperature. *Nature,* **404,** 858–861.

Gordon, C., C. Cooper, C. A. Senior, H. Banks, J. M. Gregory, T. C. Johns, J. F. B. Mitchell, and R. A. Wood, 2000: The simulation of SST, sea ice extents and ocean heat transports in a version of the Hadley Centre coupled model without flux adjustments. *Climate Dyn.,* **16,** 147–168.

Govindasamy, B., S. Thompson, A. Mirin, M. Wickett, K. Caldeira, and C. Delire, 2005: Increase of carbon cycle feedback with climate sensitivity: Results from a coupled climate and carbon cycle model. *Tellus,* **57B,** 153–163.

Hansen, J., A. Lacis, and D. Rind, 1984: *Climate Sensitivity: Analysis of Feedback Mechanisms in Climate Processes and Climate Sensitivity.* Geophys. Monogr., Vol. 29, Amer. Geophys. Union, 130–163.

Hasumi, H., and S. Emori, 2004: K-1 Coupled GCM (MIROC) description. K-1 Tech. Rep. 1, Center for Climate System Research (CCSR), University of Tokyo, National Institute for Environmental Studies (NIES), Frontier Research Center for Global Change (FRCGC), 34 pp.

Heinze, C., and E. Maier-Reimer, 1999: The Hamburg Oceanic Carbon Cycle Circulation Model Version "HAMOCC2s" for long time integrations. DKRZ Rep. 20, German Climate Computation Center, Hamburg, Germany, 71 pp.

Houghton, J. T., Y. Ding, D. J. Griggs, M. Noguer, P. J. van der Linden, X. Dai, K. Maskell, and C. A. Johnson, Eds., 2001: *Climate Change 2001: The Scientific Basis.* Cambridge University Press, 944 pp.

Houghton, R. A., and J. L. Hackler, 2002: Carbon flux to the atmosphere from land-use changes. Trends: A compendium of data on global change, Carbon Dioxide Information Analysis Center, Oak Ridge National Laboratory, U.S. Department of Energy, Oak Ridge, TN.

Hourdin, F., and Coauthors, 2005: The LMDZ4 general circulation model: Climate performance and sensitivity to param-

etrized physics with emphasis on tropical convection. *Climate Dyn.,* in press.

Huntingford, C., P. P. Harris, N. Gedney, P. M. Cox, R. A. Betts, J. Marengo, and J. H. C. Gash, 2004: Using a GCM analogue model to investigate the potential for Amazonian forest dieback in a future climate. *Theor. Appl. Climatol.,* **78,** 177–185.

Ito, A., 2005: Climate-related uncertainties in projections of the 21st century terrestrial carbon budget: Off-line model experiments using IPCC greenhouse gas scenarios and AOGCM climate projections. *Climate Dyn.,* **24,** 435–448.

——, and T. Oikawa, 2002: A simulation model of the carbon cycle in land ecosystems (Sim-CYCLE): A description based on dry-matter production theory and plot-scale validation. *Ecol. Modell.,* **151,** 147–179.

Johns, T. C., R. E. Carnell, J. F. Crossley, J. M. Gregory, J. F. B. Mitchell, C. A. Senior, S. F. B. Tett, and R. A. Wood, 1997: The second Hadley Centre coupled ocean–atmosphere GCM: Model description, spinup and validation. *Climate Dyn.,* **13,** 103–134.

Jones, C. D., and P. M. Cox, 2001: Modelling the volcanic signal in the atmospheric CO_2 record. *Global Biogeochem. Cycles,* **15,** 453–466.

——, and M. Warnier, 2004: Climate-land carbon cycle simulation of the 20th century: Assessment of HadCM3LC C4MIP phase 1 experiment. Hadley Centre Tech. Note 59, Hadley Centre, Met Office, Exeter, United Kingdom, 26 pp.

——, P. M. Cox, R. L. H. Essery, D. L. Roberts, and M. J. Woodage, 2003a: Strong carbon cycle feedbacks in a climate model with interactive CO2 and sulphate aerosols. *Geophys. Res. Lett.,* **30,** 1479, doi:10.1029/2003GL016867.

——, ——, and C. Huntingford, 2003b: Uncertainty in climate-carbon cycle projections associated with the sensitivity of soil respiration to temperature. *Tellus,* **55B,** 642–648.

——, C. McConnell, K. Coleman, P. Cox, P. Falloon, D. Jenkinson, and D. Powlson, 2004: Global climate change and soil carbon stocks; Predictions from two contrasting models for the turnover of organic carbon in soil. *Global Change Biol.,* **11,** doi:10.1111/j.1365-2486.2004.00885.x.

Joos, F., M. Bruno, R. Fink, T. F. Stocker, U. Siegenthaler, C. Le Quéré, and J. L. Sarmiento, 1996: An efficient and accurate representation of complex oceanic and biospheric models fo anthropogenic carbon uptake. *Tellus,* **48B,** 397–417.

——, I. C. Prentice, S. Sitch, R. Meyer, G. Hooss, G.-K. Plattner, S. Gerber, and K. Hasselmann, 2001: Global warming feedbacks on terrestrial carbon uptake under the Intergovernmental Panel on Climate Change (IPCC) emission scenarios. *Global Biogeochem. Cycles,* **15,** 891–907.

Jungclaus, J. H., and Coauthors, 2006: Ocean circulation and tropical variability in the coupled model ECHAM5/MPI-OM. *J. Climate*, in press.

Khodri, M., Y. Leclainche, G. Ramstein, P. Braconnot, O. Marti, and E. Cortijo, 2001: Simulating the amplification of orbital forcing by ocean feedbacks in the last glaciation. *Nature,* **410,** 570–574.

Kiehl, J. T., J. J. Hack, G. B. Bonan, B. Y. Boville, B. P. Briegleb, D. L. Williamson, and P. J. Rasch, 1996: Description of the NCAR Community Climate Model (CCM3). NCAR Tech. Note NCAR/TN-420+STR, National Center for Atmospheric Research, Boulder, CO, 152 pp.

Knorr, W., 2000: Annual and interannual CO_2 exchange of the terrestrial biosphere: Process based simulations and uncertainties. *Global Ecol. Biogeogr.,* **9,** 225–252.

——, and Coauthors, 2005: Long-term sensitivity of soil carbon turnover to warming. *Nature,* **433,** 298–301.

Krinner, G., and Coauthors, 2005: A dynamic global vegetation model for studies of the coupled atmosphere-biosphere system. *Global Biogeochem. Cycles,* **19,** GB1015.

Kucharik, C. J., and Coauthors, 2000: Testing the performance of a dynamic global ecosystem model: Water balance, carbon balance, and vegetation structure. *Global Biogeochem. Cycles,* **14,** 795–825.

Leemans, R., and Coauthors, 1998: *The IMAGE User Support System: Global Change Scenarios from IMAGE 2.1.* RIVM Publication (CD-ROM) 4815006, National Institute of Public Health and the Environment (RIVM), Bilthoven, Netherlands.

Le Quéré, C., and Coauthors, 2003: Two decades of ocean CO_2 sink and variability. *Tellus,* **55B,** 649–656.

Levitus, S., J. I. Antonov, T. P. Boyer, and C. Stephens, 2000: Warming of the world ocean. *Science,* **287,** 2225–2229.

Lloyd, J., and J. A. Taylor, 1994: On the temperature dependence of soil respiration. *Funct. Ecol.,* **8,** 315–323.

Lucht, W., and Coauthors, 2002: Climatic control of the high-latitude vegetation greening trend and Pinatubo effect. *Science,* **296,** 1687–1689.

Luo, Y. Q., S. Q. Wan, D. Hui, and L. Wallace, 2001: Acclimatization of soil respiration to warming in a tall grass prairie. *Nature,* **41,** 622–625.

Madec, G., P. Delecluse, M. Imbard, and M. Lévy, 1998: OPA 8.1 ocean general circulation model reference manual. Notes du Pôle de Modélisation 11, IPSL, Paris, France, 91 pp.

Maier-Reimer, E., 1993: Geochemical cycles in an ocean general circulation model—Preindustrial tracer distributions. *Global Biogeochem. Cycles,* **7,** 645–677.

Maltrud, M. E., R. D. Smith, A. J. Semtner, and A. J. Malone, 1998: Global eddy-resolving ocean simulations driven by 1985-1995 atmospheric winds. *J. Geophys. Res.,* **103,** 30 825–30 853.

Marland, G., T. A. Boden, and R. J. Andres, 2005: Global, regional, and national CO_2 emissions. Trends: A compendium of data on global change, Carbon Dioxide Information Analysis Center, Oak Ridge National Laboratory, U.S. Department of Energy, Oak Ridge, TN.

Marsland, S. J., H. Haak, J. H. Jungclaus, M. Latif, and F. Roeske, 2003: The Max-Planck-Institute global ocean/sea ice model with orthogonal curvilinear coordinates. *Ocean Modell.,* **5,** 91–127.

Marti, O., and Coauthors, 2005: The new IPSL climate system model: IPSL-CM4. Note du Pôle de Modélisation 26, IPSL, Paris, France, 84 pp.

Martin, J. H., G. A. Knaueer, D. M. Karl, and W. W. Broenkow, 1987: VERTEX: Carbon cycling in the northeast Pacific. *Deep-Sea Res.,* **34,** 267–285.

Matthews, H. D., A. J. Weaver, K. J. Meissner, N. P. Gillett, and M. Eby, 2004: Natural and anthropogenic climate change: Incorporating historical land cover change, vegetation dynamics and the global carbon cycle. *Climate Dyn.,* **22,** 461–479.

——, ——, and ——, 2005a: Terrestrial carbon cycle dynamics under recent and future climate change. *J. Climate,* **18,** 1609–1628.

——, M. Eby, A. J. Weaver, and B. J. Hawkins, 2005b: Primary productivity control of simulated carbon cycle-climate feed-

backs. *Geophys. Res. Lett.,* **32,** L14708, doi:10.1029/2005GL022941.

McGuire, A. D., J. M. Melillo, L. M. Joyce, D. M. Kicklighter, A. L. Grace, B. Moore III, and C. J. Vorosmarty, 1992: Interactions between carbon and nitrogen dynamics in estimating net primary productivity for potential vegetation in North America. *Global Biogeochem. Cycles,* **6,** 101–124.

Meehl, G. A., W. M. Washington, J. M. Arblaster, and A. Hu, 2004: Factors affecting climate sensitivity in global coupled models. *J. Climate,* **17,** 1584–1596.

Meissner, K. J., A. J. Weaver, H. D. Matthews, and P. M. Cox, 2003: The role of land-surface dynamics in glacial inception: A study with the UVic Earth System Climate Model. *Climate Dyn.,* **21,** 515–537.

Monsi, M., and T. Saeki, 1953: Über den Lichtfaktor in den Pfanzengesellschaften und seine Bedeutung für die Stoffproduktion. *Japan. J. Botany,* **14,** 22–52.

——, and ——, 2005: On the factor light in plant communities and its importance for matter production. *Ann. Botany (London),* **95,** 549–567.

Murphy, J. M., D. M. H. Sexton, D. N. Barnett, G. S. Jones, M. J. Webb, M. Collins, and D. A. Stainforth, 2004: Quantification of modelling uncertainties in a large ensemble of climate change simulations. *Nature,* **430,** 768–772.

Najjar, R. G., and J. C. Orr, cited 1999: Biotic How-To. Revision 1.7, Ocean Carbon-cycle Model Intercomparison Project (OCMIP). [Available online at http://www.ipsl.jussieu.fr/OCMIP/phase2/simulations/Biotic/HOWTO-Biotic.html.]

——, J. L. Sarmiento, and J. R. Toggweiler, 1992: Downward transport and fate of organic matter in the ocean: Simulations with a general circulation model. *Global Biogeochem. Cycles,* **6,** 45–76.

Neelin, J. D., and N. Zeng, 2000: The first quasi-equilibrium tropical circulation model—Formulation. *J. Atmos. Sci.,* **57,** 1741–1766.

New, M., M. Hulme, and P. D. Jones, 1999: Representing twentieth-century space–time climate variability. Part I: Development of a 1961–90 mean monthly terrestrial climatology. *J. Climate,* **12,** 829–856.

——, ——, and ——, 2000: Representing twentieth-century space–time climate variability. Part II: Development of 1901–96 monthly grids of terrestrial surface climate. *J. Climate,* **13,** 2217–2238.

Nowak, R. S., D. S. Ellsworth, and S. D. Smith, 2004: Functional responses of plants to elevated atmospheric CO_2—Do photosynthetic and productivity data from FACE experiments support early predictions? *New Phytol.,* **162,** 253–280.

Oschlies, A., 2001: Model-derived estimates of new production: New results point towards lower values. *Deep-Sea Res.,* **48,** 2173–2197.

Palmer, J. R., and I. J. Totterdell, 2001: Production and export in a global ocean ecosystem model. *Deep-Sea Res.,* **48,** 1169–1198.

Parton, W. J., and Coauthors, 1993: Observations and modeling of biomass and soil organic matter dynamics for the grassland biome worldwide. *Global Biogeochem. Cycles,* **7,** 785–809.

Petoukhov, V., A. Ganopolski, V. Brovkin, M. Claussen, A. Eliseev, C. Kubatzki, and S. Rahmstorf, 2000: CLIMBER-2: A climate system model of intermediate complexity. Part I: Model description and performance for present climate. *Climate Dyn.,* **16,** 1–17.

——, and Coauthors, 2005: EMIC Intercomparison Project (EMIP-CO2): Comparative analysis of EMIC simulations of climate, and of equilibrium and transient responses to atmospheric CO_2 doubling. *Climate Dyn.,* **25,** 363–385.

Prentice, I. C., and Coauthors, 2001: The carbon cycle and atmospheric carbon dioxide. *Climate Change 2001: The Scientific Basis,* J. T. Houghton et al., Eds., Cambridge University Press, 183–237.

Raich, J., and W. Schlesinger, 1992: The global carbon dioxide flux in soil respiration and its relationship to vegetation and climate. *Tellus,* **44,** 81–99.

Randerson, J. T., M. V. Thompson, T. J. Conway, I. Y. Fung, and C. B. Field, 1997: The contribution of terrestrial sources and sinks to trends in the seasonal cycle of atmospheric carbon dioxide. *Global Biogeochem. Cycles,* **11,** 535–560.

Roeckner, E., and Coauthors, 2003: The general circulation model ECHAM5. Part I: Model description. Max Planck Institute for Meteorology Rep. 349, Hamburg, Germany, 127 pp.

Sarmiento, J. L., T. M. C. Hughes, R. J. Stouffer, and S. Manabe, 1998: Simulated response of the ocean carbon cycle to anthropogenic climate warming. *Nature,* **393,** 245–249.

Schimel, D. S., and Coauthors, 2001: Recent patterns and mechanisms of carbon exchange by terrestrial ecosystems. *Nature,* **414,** 169–172.

Sitch, S., and Coauthors, 2003: Evaluation of ecosystem dynamics, plant geography and terrestrial carbon cycling in the LPJ dynamic global vegetation model. *Global Change Biol.,* **9,** 161–185.

——, V. Brovkin, W. von Bloh, D. van Vuuren, B. Eickhout, and A. Ganopolski, 2005: Impacts of future land cover changes on atmospheric CO_2 and climate. *Global Biogeochem. Cycles,* **19,** GB2013, doi:10.1029/2004GB002311.

Six, K. D., and E. Maier-Reimer, 1996: Effects of plankton dynamics on seasonal carbon fluxes in an ocean general circulation model. *Global Biogeochem. Cycles,* **10,** 559–583.

Thompson, S. L., B. Govindasamy, A. Mirin, K. Caldeira, C. Delire, J. Milovich, M. Wickett, and D. Erickson, 2004: Quantifying the effects of CO_2-fertilized vegetation on future global climate. *Geophys. Res. Lett.,* **31,** L23211, doi:10.1029/2004GL021239.

Washington, W. M., and Coauthors, 2000: Parallel Climate Model (PCM) control and transient simulations. *Climate Dyn.,* **16,** 755–774.

Weaver, A. J., and Coauthors, 2001: The UVic earth system climate model: Model description, climatology and applications to past, present and future climate. *Atmos.–Ocean,* **39,** 361–428.

Wetzel, P., A. Winguth, and E. Maier-Reimer, 2005: Sea-to-air CO_2 fluxes from 1948 to 2003: A model study. *Global Biogeochem. Cycles,* **19,** GB2005, doi:10.1029/2004GB002339.

Zeng, N., 2003: Glacial-interglacial atmospheric CO_2 changes—The Glacial Burial Hypothesis. *Adv. Atmos. Sci.,* **20,** 677–693.

——, J. D. Neelin, and C. Chou, 2000: A quasi-equilibrium tropical circulation model—Implementation and simulation. *J. Atmos. Sci.,* **57,** 1767–1796.

——, H. Qian, E. Munoz, and R. Iacono, 2004: How strong is carbon cycle-climate feedback under global warming? *Geophys. Res. Lett.,* **31,** L20203, doi:10.1029/2004GL020904.

——, A. Mariotti, and P. Wetzel, 2005: Terrestrial mechanisms of interannual CO_2 variability. *Global Biogeochem. Cycles,* **19,** GB1016, doi:10.1029/2004GB002273.